NJC

ROYAL SOCIETY OF CHEMISTRY

PAPER

View Article Online
View Journal | View Issue

Cite this: *New J. Chem.*, 2023, **47**, 18442

Synthesis of Pt(II) phosphinocarboxylate complexes with auxiliary arylcarbene ligands and factors that control their stereochemistry†

Filip Horký,[a] Johannes Soellner,[b] Jiří Schulz,[a] Ivana Císařová,[a] Thomas Strassner *[b] and Petr Štěpnička *[a]

Received 9th August 2023,
Accepted 20th September 2023

DOI: 10.1039/d3nj03729k

rsc.li/njc

Orthoplatinated complexes [Pt(C^C*)(acac)] (**1**^{R}), in which C^C* is orthoplatinated 3-R-1-phenyl-1*H*-benzo[*d*]imidazol-2-ylidene and R = Me and Ph, reacted with 1′-(diphenylphosphino)ferrocene-1-carboxylic acid (Hdpf) under protonation of the acetylacetonate ligand (acac) to produce the corresponding phosphinocarboxylate bischelate complexes [Pt(C^C*)(dpf-κ^2*O*,*P*)] (**2**^{R}) as single isomers with *trans*-P,C(carbene) geometry. The compounds were fully characterized by elemental analysis, spectroscopic methods, single-crystal X-ray diffraction analysis, and cyclic voltammetry. In addition, DFT calculations were used to determine differences in energy and the bonding situation between **2**^{R} and the hypothetical geometric isomers **3**^{R} with a *trans*-P,C(phenyl) arrangement. The experimental and theoretical results are consistent with the antisymbiosis effect observed in complexes of soft metal ions, namely with weakening of Pt–C bonds by strongly *trans*-influencing ligands.

Introduction

Reactions between Pd and Pt-acetylacetonate (acac) complexes and Brønsted acids typically proceed under protonation of the acac ligand, which leads to its decoordination and liberation of two coordination sites at the metal.[1] In this way, the readily accessible acetylacetonate complexes can serve as convenient precursors of diverse transition metal compounds.[2] Examples include products obtained through reactions between palladium(II) acetylacetonate and imidazolium salts to produce carbene complexes[3] as well as analogous reactions with oxalic amidinates,[4] 2,5-diamino-1,4-benzoquinonediimine,[5] 1-(isoquinolin-1-yl)-2-naphtholes,[6] and porphyrins bearing enaminoketone moieties at the periphery,[7] or reactions between the corresponding platinum(II) complex and secondary phosphine oxides[8] or benzoquinonediimines.[9]

Reactions of acetylacetonate complexes with protic difunctional proligands (X^YH) that produce X,Y-chelate complexes are particularly attractive. For instance, the Pd-acetylacetonate complex [(L^{NC})Pd(acac)], where L^{NC} stands for orthometallated 2-(dimethylamino-κ*N*)phenyl-κ*C*^{1} ligand, reacted with amino acids to generate *N*,*O*-chelate complexes of the type [(L^{NC})-Pd(NH$_2$CH(R)CO$_2$-κ^2*N*,*O*)].[10] In our research, we used a similar approach to prepare P,O-chelate complexes from phosphinoferrocene carboxylic and phosphonic acids.[11,12] In these reactions, we consistently observed the formation of a single isomer in which the phosphine moiety and phenyl group from the L^{NC} ligand (as the donors with the largest *trans* influence[13]) mutually occupy *cis* positions, in line with the antisymbiosis (or transphobia) concept.[14] Now we considered analogous complexes obtained from cyclometallated Pt(II)-carbene complexes [(C^C*)Pt(acac)] (**1** in Scheme 1) because their orthoplatinated C^C* ligands less significantly differentiate the two remaining coordination sites by *trans* influence,[15] which can result in dichotomy in reactivity. Compounds **1** were studied as

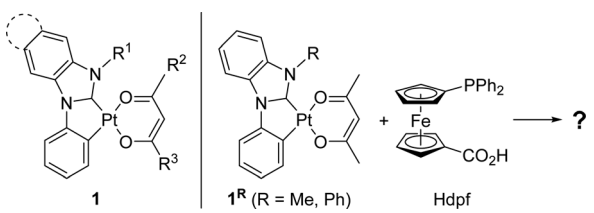

Scheme 1 General formula of compounds **1** and reactions investigated in this work.

[a] *Department of Inorganic Chemistry, Faculty of Science, Charles University, Hlavova 2030, 128 40 Prague, Czech Republic. E-mail: stepnic@natur.cuni.cz*
[b] *Physikalische Organische Chemie, Technische Universität Dresden, Bergstrasse 66, 01069 Dresden, Germany. E-mail: thomas.strassner@chemie.tu-dresden.de*

† Electronic supplementary information (ESI) available: Summary of crystallographic parameters, additional structure diagrams, electrochemical data and results from IBO analysis, copies of the NMR spectra, and cartesian coordinates for the DFT-optimized structures of **2**^{R} and **3**^{R}. CCDC 2284526 and 2284527. For ESI and crystallographic data in CIF or other electronic format see DOI: https://doi.org/10.1039/d3nj03729k

tuneable photoluminescent materials[16] but have only rarely been used as synthetic precursors thus far.

In this contribution we build upon our recent research focused on the reactions of type **1** complexes with α-donor substituted acetic acids,[17] now aiming on the reactions with 1′-(diphenylphosphino)ferrocene-1-carboxylic acid (Hdpf).[18] In particular, we report the results of our reactivity studies using two Pt(II) precursors, detailed structural characterization of the resulting complexes, and DFT calculations focused on the differences in energy and bonding situation between the product isomers.

Results and discussion

Syntheses and structural characterization

Reactions of complexes $\mathbf{1^R}$ with Hdpf produced the respective phosphinocarboxylate complexes $\mathbf{2^R}$ with *trans*-P,C(carbene) geometry (Scheme 2), which were isolated in approximately 70% yields. In these isomers, the phosphine moiety and the aryl group of the C^C* ligand (C), which exerts a higher *trans* influence than the carbene moiety (C*),[15] occupy mutually *cis* positions. Isomers $\mathbf{3^R}$ with the *trans*-P,C(phenyl) arrangement have not been detected.

The compounds were characterized by multinuclear NMR and IR spectroscopy, mass spectrometry, and elemental analysis. In addition, the solid-state structures of $\mathbf{2^{Me}}\cdot CH_2Cl_2$ and $\mathbf{2^{Ph}}\cdot$1/2AcOEt were determined by single-crystal X-ray diffraction analysis. In their ^{1}H and ^{13}C NMR spectra, the complexes showed the expected signals, including the diagnostic resonances due to carboxylate and carbene carbons at δ_C 175.82 and 178.48 ppm for $\mathbf{2^{Me}}$ and at δ_C 174.27 and 178.24 ppm for $\mathbf{2^{Ph}}$ (the carbene resonances were observed as doublets due to coupling with the proximal phosphine moiety, $^2J_{PC}$ = 145–146 Hz). The IR spectra displayed intense bands at 1578 cm^{-1} attributable to the ν_{as} mode of the carboxylate ligands. The ^{31}P NMR resonances were observed at 19.4 ($\mathbf{2^{Me}}$) and 18.9 ($\mathbf{2^{Ph}}$) ppm as singlets with ^{195}Pt satellites ($^1J_{PtP}$ = 2964 and 2990 Hz).[19] The compounds showed no significant luminescence in PMMA matrix at room temperature (quantum yields < 5%), which is indeed in line with our previous observations[20] and can be rationalised by quenching by the ferrocene moiety.[21]

The structures of the complexes are depicted in Fig. 1, and Table 1 provides selected geometric parameters. The compounds present square-planar coordination around the Pt(II) centres. The Pt-donor distances are similar to those determined for precursors $\mathbf{1^R}$ (ref. 22) and the phosphinocarboxylate

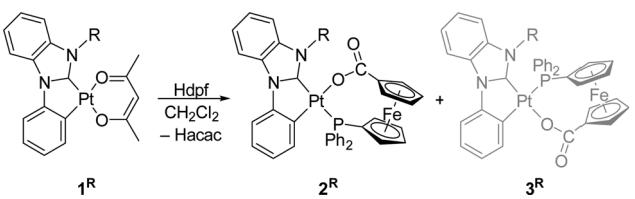

Scheme 2 Synthesis of complexes $\mathbf{2^R}$ (R = Me, Ph). Isomeric compounds $\mathbf{3^R}$ were not detected.

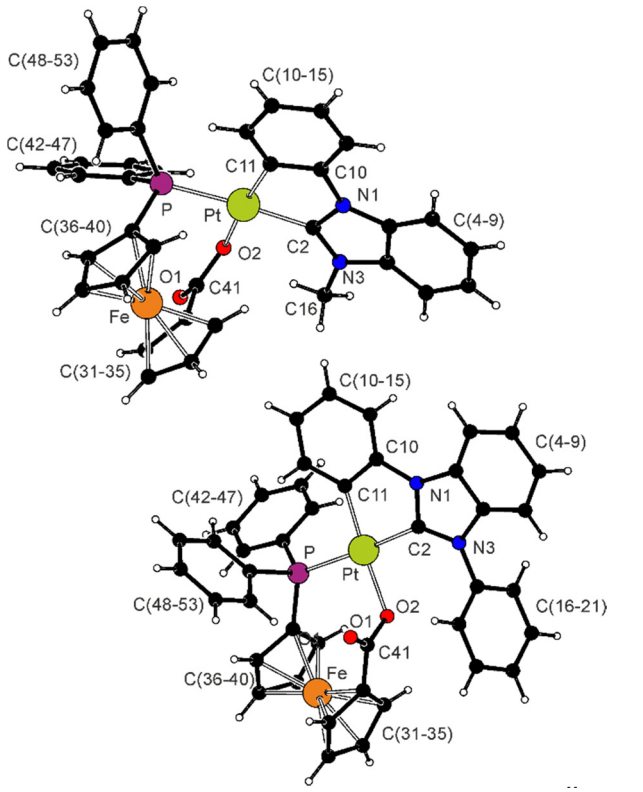

Fig. 1 Views of the complex molecules in the crystal structures of $\mathbf{2^{Me}}\cdot CH_2Cl_2$ (top) and $\mathbf{2^{Ph}}\cdot$1/2AcOEt (bottom). Displacement ellipsoid plots are available in the ESI.†

Table 1 Selected distances and angles for $\mathbf{2^{Me}}\cdot CH_2Cl_2$ and $\mathbf{2^{Ph}}\cdot$1/2AcOEt (in Å and deg)

Parameter[a]	$\mathbf{2^{Me}}\cdot CH_2Cl_2$	$\mathbf{2^{Ph}}\cdot$1/2AcOEt
Pt–P	2.3305(5)	2.3192(7)
Pt–O2	2.117(1)	2.093(1)
Pt–C2	2.016(2)	2.004(2)
Pt–C11	2.011(2)	2.016(2)
P–Pt–O2	86.27(3)	87.08(4)
P–Pt–C11	100.16(5)	97.11(6)
C2–Pt–C11	79.83(7)	79.70(8)
C2–Pt–O2	93.98(6)	96.10(7)
Fe–C (range)[b]	2.026(2)–2.060(2)	2.022(2)–2.069(2)
Tilt	1.0(1)	6.4(1)
τ	−12.3(1)	−4.0(1)
P–C36	1.796(2)	1.824(2)
P–C42/P–C48	1.827(2)/1.836(2)	1.823(2)/1.825(2)
C41–O1/C41–O2	1.235(2)/1.290(2)	1.234(2)/1.291(2)
O1–C41–O2	122.2(2)	126.1(2)

[a] Tilt is the dihedral angle of the least-square cyclopentadienyl planes C(31–35) and (C36–40), τ denotes the torsion angle C31–Cg1–Cg2–C36, where Cg2 and Cg2 stand for the centroids of the rings C(31–35) and (C36–40), respectively. [b] The range of the Fe–C(31–40) bonds.

complex $[(\mathbf{L^{Ph}})Pt(Ph_2PCH_2CO_2\text{-}\kappa^2O,P)]$, where $\mathbf{L^{Ph}}$ stands for the C^C* ligand arising from $\mathbf{1^{Ph}}$;[17] the differences in the parameters obtained for $\mathbf{2^{Me}}$ and $\mathbf{2^{Ph}}$ are only small and can be explained by steric factors. The benzimidazol-2-ylidene fragments and the platinated benzene rings are almost coplanar (the interplanar angles are 9.06(7)° and 2.63(9)° in $\mathbf{2^{Me}}$ and

2^{Ph}, respectively), while the phenyl substituent in 2^{Ph} is twisted to minimize steric congestion (interplanar angle: 68.65(8)°). The ferrocene moieties exhibit negligible tilting and adopt conformations near to eclipsed (see τ angles in Table 1). The carboxylate groups retain partly localized character (C41–O1 < C41–O2) and are twisted from the planes of their parent cyclopentadienyl rings (by 25.9(2)° and 22.5(2)° in 2^{Me} and 2^{Ph}, respectively) to ensure that O2 approaches the Pt centre.

The redox properties of complexes 2^{R} were studied by cyclic voltammetry at a glassy carbon disc electrode using dichloromethane solutions containing $Bu_4N[PF_6]$ as the supporting electrolyte. The compounds displayed similar but rather complicated behaviour (Fig. 2). Initially, they underwent diffusion-controlled oxidation [indicated by the anodic peak potential (i_{pa}) increasing linearly with $\nu^{1/2}$, $i_{pa} \propto \nu^{1/2}$, where ν is scan rate], which was essentially reversible when scanned separately (*i.e.*, when the switching potential was set after the first oxidation) *and* at relatively faster scan rates ($\nu \geq 100$ mV s^{-1}). At slower scan rates, however, the reversibility markedly decreased (Fig. 3), suggesting that the redox change is followed by chemical reaction(s) that convert the oxidized molecule into other species. The oxidation occurred at $E^{\circ\prime}$ 0.26 V for 2^{Me} and at 0.21 V for 2^{Ph} ($E^{\circ\prime}$ determined at ν = 100 mV s^{-1}, when the redox change appears essentially reversible; values *vs.* ferrocene/ferrocenium standard), which is more positive than for Hdpf (0.31 V in MeCN).[18a] Considering the nature of HOMO (Fig. 4), the oxidation was attributed to ferrocene/ferrocenium redox transition (*vide infra*).

After the scan range was expanded towards more positive potentials, additional weaker redox waves were observed (Fig. 2). These redox transitions were associated with ill-defined, irreversible reduction steps and differed for the two compounds. In the cathodic region, no defined redox waves were detected. However, after scanning towards positive potentials (oxidation), weak irreversible waves were observed in the cathodic region, attributable to decomposition products.

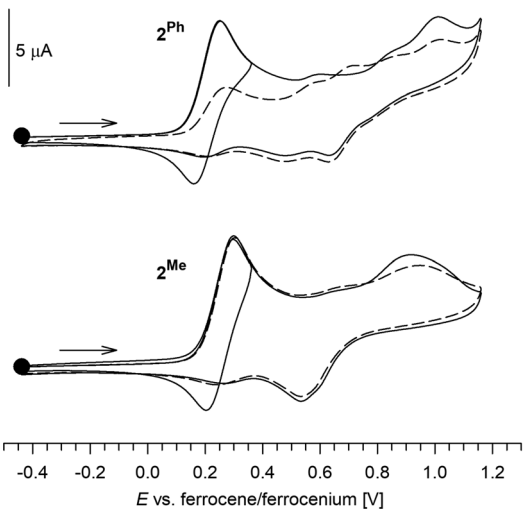

Fig. 2 Cyclic voltammograms of 2^{Me} and 2^{Ph} as recorded at a glassy carbon electrode in dichloromethane at a 100 mV s^{-1} scan rate. The second scan is shown by a dashed line.

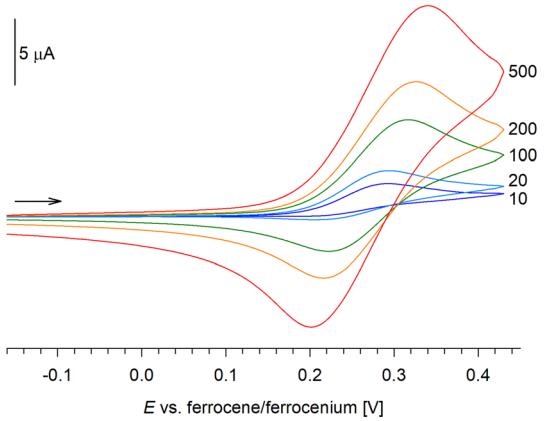

Fig. 3 Cyclic voltammograms of 2^{Me} recorded at varying scan rate (values in mV s^{-1}). A similar Figure for 2^{Ph} is available in ESI.†

DFT calculations

The electronic structures of 2^{R} and 3^{R} were studied by computational methods (DFT) at the B3LYP(d3bj)/6-311+G(d,p):LanL2TZ(Pt) level of theory. The frontier orbitals of 2^{Me} and 2^{Ph} exhibit almost identical spatial contours (Fig. 4). Their composition was analysed by the Natural Atomic Orbitals (NAO) approach, revealing that the HOMO of both complexes is localized almost exclusively on the ferrocene ligand and consists mainly of the iron 3d orbitals (≈85%) with smaller contributions from the carbon 2p orbitals constituting the π-system of the cyclopentadienyl rings (≈11%). This result already suggested that the initial electrochemical oxidation of

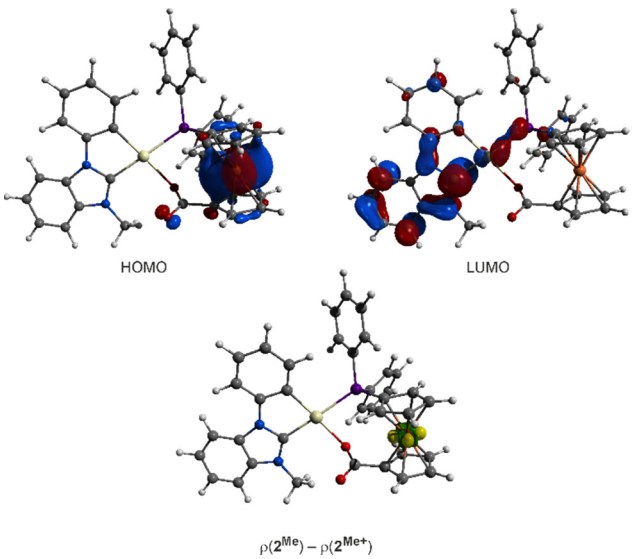

Fig. 4 (top) Frontier orbitals of 2^{Me} (contour maps with isosurfaces at ±0.04 a.u.) at the B3LYP(d3bj)/6-311+G(d,p):LanL2TZ(Pt) level of theory, and (bottom) the electron difference map $\rho(2^{Me})-\rho(2^{Me+})$ mapped at the equilibrium geometry of 2^{Me} (isosurface at ±0.02 a.u.). A similar diagram for 2^{Ph} is available in the ESI.†

Table 2 Energy differences (ΔG) between isomers $\mathbf{2^R}$ and $\mathbf{3^R}$ (in kcal mol^{-1}) at different levels of theory[a]

Method	$\mathbf{2^{Me}}$/$\mathbf{3^{Me}}$	$\mathbf{2^{Ph}}$/$\mathbf{3^{Ph}}$
B3LYP/6-31G(d)	−7.51	−6.69
B3LYP/6-311+G(d,p)	−7.76	−7.08
B3LYP/6-311+G(d,p)+dispersion	−8.45	−4.05
B3LYP/6-311+G(d,p)+PCM	−5.22	−5.75

[a] Determined as $\Delta G = G(\mathbf{2^R}) - G(\mathbf{3^R})$ at 298 K. For details, see Experimental.

$\mathbf{2^R}$ is a ferrocene-centred process. This was further corroborated by following the change in the electron density associated with electron removal, $\rho(\mathbf{2^R})$–$\rho(\mathbf{2^{R+}})$, mapped at the equilibrium geometry of $\mathbf{2^R}$,[23] which was located exclusively at the iron atom (Fig. 4).

Conversely, the LUMO in both compounds is highly delocalized, comprising mostly the π-system of the benzimidazole moiety with contributions from the vacant p-orbital of the carbene atom (≈25%), the platinum ion (≈15%, 6p and 5d) and the phosphorus atom (≈3%, 3p).

Consistent with the experimental observation, the computations suggested that $\mathbf{2^R}$ are the thermodynamically favoured isomers (Table 2). The trend is maintained even when the dispersion effects are included in the calculations, albeit with a different impact on the two compound pairs. The inclusion of solvation phenomena significantly decreased the energy difference between the isomers to approximately 5 kcal mol^{-1}. The slightly higher energy difference that was estimated for $\mathbf{2^{Ph}}$/$\mathbf{3^{Ph}}$ can be rationalized by steric factors, namely, by possible steric congestion in $\mathbf{3^{Ph}}$, in which the PPh_2 group and the phenyl substituent are directed towards each other.[24]

The Pt-donor distances calculated for $\mathbf{2^R}$ reasonably corresponded with the experimental values (Table 3). More importantly, a comparison of the data calculated for $\mathbf{2^R}$ and the hypothetical isomers $\mathbf{3^R}$ revealed longer Pt–P and shorter Pt–O bonds for the latter isomers, in line with the stronger *trans* influence of the Pt-bound phenyl group. In contrast, the Pt–C bonds did not differ significantly in the two isomers.

Furthermore, the lower Mulliken charges at platinum in $\mathbf{2^R}$ (*cf.* $\mathbf{2^{Me}}$/$\mathbf{3^{Me}}$ 0.579/0.665, and $\mathbf{2^{Ph}}$/$\mathbf{3^{Ph}}$ 0.428/0.507) suggested a stronger P → Pt donation in these isomers. The charges at the Pt-bound carboxylate oxygens were −0.338/−0.128 for $\mathbf{2^{Me}}$/$\mathbf{3^{Me}}$ and −0.125/−0.045 for $\mathbf{2^{Ph}}$/$\mathbf{3^{Ph}}$. Compared to the predominantly covalent Pt–P bonds, the Pt–O bonds are more ionic and thus less sensitive to length variation.

Table 3 Comparison of the calculated and experimental Pt-donor distances (in Å)[a]

Complex	Pt–P	Pt–O	Pt–C(carbene)	Pt–C(Ph)
$\mathbf{2^{Me}}$ (exp.)	2.3305(5)	2.117(1)	2.016(2)	2.011(2)
$\mathbf{2^{Me}}$ (DFT)	2.437	2.189	2.005	2.025
$\mathbf{3^{Me}}$ (DFT)	2.519	2.100	1.978	2.027
$\mathbf{2^{Ph}}$ (exp.)	2.3192(7)	2.093(1)	2.004(2)	2.016(2)
$\mathbf{2^{Ph}}$ (DFT)	2.439	2.172	1.991	2.029
$\mathbf{3^{Ph}}$ (DFT)	2.541	2.100	1.974	2.024

[a] Experimental values are reproduced from Table 1. Calculated data at the B3LYP/6-311+G(d,p) level of theory.

The bonding situation in isomers **2** and **3** was further analysed using the intrinsic bond orbital (IBO) approach,[25] which provides a representation of the Kohn–Sham wavefunction in terms of the more intuitive localized orbitals. A comparison of the IBOs representing the donor–acceptor interactions in $\mathbf{2^{Me}}$ and $\mathbf{3^{Me}}$ (Fig. 5) clearly shows the mutual *trans*-influence of the donor atoms in both isomers. The stronger σ-donor ligands tend to polarize the electron density of the M–L bond towards the *trans*-positioned ligand. Thus, the coordination of the phosphine group in $\mathbf{3^{Me}}$ (as expressed by the assigned partial charges: P 1.73/Pt 0.18) is weakened compared to that of $\mathbf{2^{Me}}$ (P 1.67/Pt 0.26) due to the strong *trans* influence of the X-type[26] phenyl ligand. In contrast, the carbene-platinum bond appears insensitive to the influence of the phosphine group in the *trans* position ($\mathbf{2^{Me}}$: C 1.53/Pt 0.41 *vs.* $\mathbf{3^{Me}}$: C 1.51/Pt 0.43) and the Pt → P back-bonding is negligible, although slightly enhanced in $\mathbf{2^{Me}}$ (apparently at the expense of the weakened back-donation to the carbene ligand). The preferred mutual arrangement of the coordinated chelating ligands is thus *trans*-P,C(carbene), which reflects the relative σ-donor strength of the coordinated donor atoms and places the most ionic (Pt–O) and the most covalent coordination bonds (Pt–C^{Ph}) opposite to each other.

Conclusions

Compounds [Pt(C^C*)(acac)] (**1**), where C^C*stands for a chelating benzimidazole-2-ylidene ligand with an orthoplatinated phenyl substituent, react cleanly with 1′-(diphenylphosphino)-ferrocene-1-carboxylic acid (Hdpf) under proton transfer to the acetylacetonate and coordination of the formed dpf^- anion as an *O*,*P*-chelating ligand. Of the two possible geometric isomers, which differ by the mutual orientation of the two chelating ligands, only the isomer with a *trans*-P,C(carbene) arrangement was detected and isolated due to a destabilizing effect exhibited by strongly *trans*-influencing donor moieties from the chelating ligands (*viz.*, the phenyl and phosphine). The analysis of the bonding situation by DFT calculations and the IBO approach revealed a weakening of the covalent Pt–C interactions by the strongly donating *trans*-ligand, in line with the transphobia concept.

Experimental

Materials and methods

All syntheses were performed under an argon atmosphere using standard Schlenk techniques. Complexes $\mathbf{1^{Me}}$ and $\mathbf{1^{Ph}}$ (ref. 22) and Hdpf[18a] were prepared according to procedures described in literature. Anhydrous dichloromethane was obtained from a Pure Solv MD5 solvent purification system (Innovative Technology, USA). Solvents used for workup and chromatography (Lach-Ner, Czech Republic) were utilized without further purification.

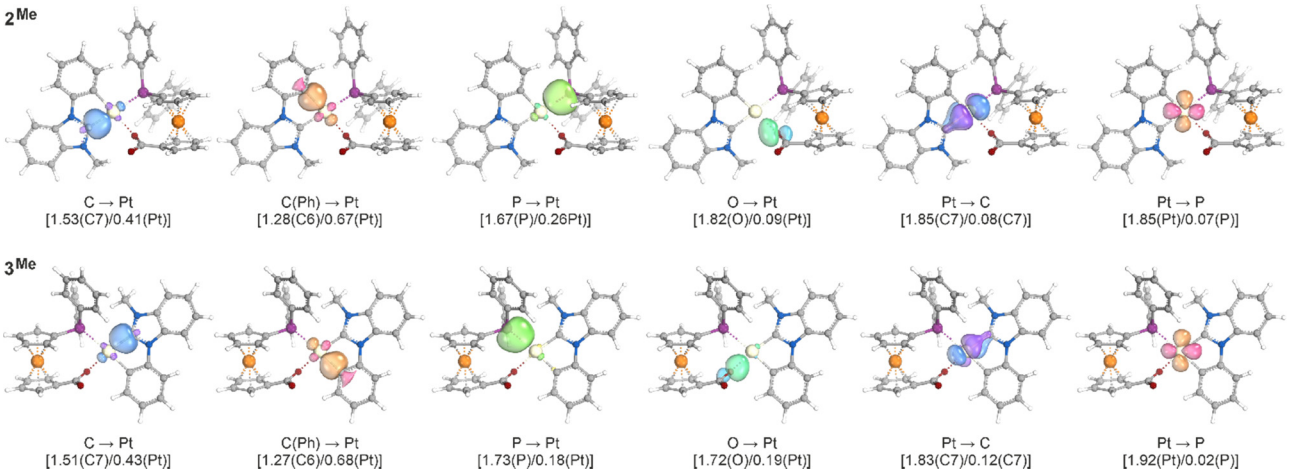

Fig. 5 Selected intrinsic bond orbitals (IBOs) of $\mathbf{2^{Me}}$ and $\mathbf{3^{Me}}$. Values in parentheses indicate the fraction of bonding electrons assigned to the individual atoms. The carbon atoms are labelled as in the crystal structure. Similar diagrams for $\mathbf{2^{Ph}}$ and $\mathbf{3^{Ph}}$ are available in the ESI.†

NMR spectra were recorded with a Varian INOVA 400 spectrometer operating at 399.95, 100.58, and 161.90 MHz for ^{1}H, ^{13}C, and ^{31}P, respectively. The chemical shifts (δ in ppm) are expressed relative to $SiMe_4$ as an internal standard (^{1}H and ^{13}C) and to 85% aqueous H_3PO_4 as an external reference (^{31}P). In addition to the standard notation of signal multiplicity,[27] vt and vq are used to denote virtual triplets and quartets arising from AA′BB′ and AA′BB′X (A, B = ^{1}H; X = ^{31}P) spin systems constituted by the ferrocene cyclopentadienyl rings, respectively. ESI mass spectra were recorded with an AmaZon SL (Bruker) ion trap spectrometer using samples dissolved in HPLC-grade acetonitrile. IR spectra were recorded in diffuse reflectance mode (DRIFTS) using a Nicolet FTIR 205 spectrometer. The emission spectra were recorded with a Hamamatsu Quantaurus spectrometer, model C9920-02, using samples dispersed in PMMA matrix. Elemental analyses were performed with a PerkinElmer 2400 Series II CHNS/O analyser. The presence of residual solvent was confirmed by NMR analysis.

Electrochemical measurements were performed at ambient temperature using an μAUTOLAB III instrument (Eco Chemie) and a three-electrode cell equipped with a glassy carbon disc (2 mm diameter) working electrode, a platinum sheet auxiliary electrode, and a Ag/AgCl (3 M KCl) reference electrode. The samples were dissolved in anhydrous dichloromethane to generate a solution containing 1 mM of the analysed compounds and 0.1 M $Bu_4N[PF_6]$ as the supporting electrolyte. The solutions were deaerated with argon before measurements and then maintained under an argon blanket. Decamethylferrocene (Alfa-Aesar) was added as an internal standard during the final scans, and the redox potentials were subsequently converted to the ferrocene/ferrocenium scale by subtracting 0.548 V.[28]

Syntheses

Synthesis of 2Me. Compound $\mathbf{1^{Me}}$ (35 mg, 70 μmol) and Hdpf (29 mg, 70 μmol) were dissolved in anhydrous dichloromethane (13 mL), and the resulting mixture was stirred at ambient temperature overnight. Then, the mixture was concentrated, and the residue was purified by filtration through a short silica gel column and eluted with dichloromethane-methanol (10 : 1). A single orange band was collected and evaporated, leaving solvated complex $\mathbf{2^{Me}}$ as an orange solid. Yield of $\mathbf{2^{Me}}\cdot 1/2CH_2Cl_2$: 41 mg (72%). The single crystal of $\mathbf{2^{Me}}\cdot CH_2Cl_2$ used for structure determination was grown from dichloromethane/isohexane.

^{1}H NMR (399.95 MHz, $CDCl_3$): δ 4.22 (vt, J' = 1.9 Hz, 2H, fc), 4.37 (s, 3H, Me), 4.37–4.39 (m, 2H, fc), 4.51–4.52 (m, 2H, fc), 5.33 (vt, J' = 1.9 Hz, 2H, fc), 6.35 (td, J = 7.5, 1.3 Hz, 1H, C_6H_4), 6.56 (ddd with ^{195}Pt satellites, $J_{PtC} \approx 60$ Hz, J = 7.8, 2.3, 1.3 Hz, 1H, C_6H_4), 6.99 (td, J = 7.5, 1.3 Hz, 1H, C_6H_4), 7.32–7.59 (m, 10H, PPh_2), 7.80–7.86 (m, 4H, C_6H_4), 8.04–8.09 (m, 1H, C_6H_4). ^{13}C{^{1}H} NMR (100.58 MHz, $CDCl_3$): δ 32.55 (s, Me), 70.97 (s, CH of fc), 71.75 (d, $^{1}J_{PC}$ = 57 Hz, C–P of fc), 72.20 (d, J_{PC} = 7 Hz, CH of fc), 72.62 (s, CH of fc), 75.44 (d, J_{PC} = 11 Hz, CH of fc), 80.54 (s, *C*-COO of fc), 111.49 (s, CH of C_6H_4), 111.88 (s, CH of C_6H_4), 112.31 (s with ^{195}Pt satellites, $J_{PtC} \approx 30$ Hz, CH of C_6H_4), 118.95 (d, $^{3}J_{PC}$ = 6 Hz, C–N of C_6H_4), 123.62 (s, CH of C_6H_4), 123.93 (br s with ^{195}Pt satellites, $J_{PtC} \approx 60$ Hz, 2× CH of C_6H_4), 125.01 (s, CH of C_6H_4), 128.33 (d, J_{PC} = 11 Hz, CH of PPh_2), 130.45 (s, CH of PPh_2), 132.20 (d, $^{1}J_{PC}$ = 52 Hz, C–P of PPh_2), 134.34 (d, J_{PC} = 12 Hz, CH of PPh_2), 135.92 (d, $^{4}J_{PC}$ = 6 Hz, C–N of C_6H_4), 139.35 (d, $^{4}J_{PC}$ = 8 Hz, CH of C_6H_4), 148.78 (d, $^{2}J_{PC}$ = 2 Hz, C–Pt of C_6H_4), 175.82 (s, COO), 178.48 (d, $^{2}J_{PC}$ = 145 Hz, NCN). The signal due to the second C–N of C_6H_4 was not detected. ^{31}P{^{1}H} NMR (161.90 MHz, $CDCl_3$): δ 19.4 (s with ^{195}Pt satellites, $^{1}J_{PtP}$ = 2964 Hz, PPh_2). IR (DRIFTS): ν = 3409 br m, 3053 br m, 2953 br m, 1598 s, 1478 s, 1436 s, 1380 s, 1362 m, 1324 s, 1247 w, 1178 m, 1098 m, 1052 m, 1030 m, 999 w, 922 w, 804 w, 791 w, 749 s, 696 s, 673 w, 631 w, 540 m, 522 s, 507 s, 476 s cm^{-1}. HRMS (ESI+) calc. for $C_{37}H_{30}FeN_2O_2PPt$ ($[M + H]^+$): 816.1037, found: 816.1032. Anal. calc. for $C_{37}H_{29}FeN_2O_2PPt\cdot 1/2CH_2Cl_2$ (833.4): C 53.67, H 3.56, N 3.37%. Found: C 53.66, H 3.38, N 3.40%.

Synthesis of $\mathbf{2^{Ph}}$. Complex $\mathbf{1^{Ph}}$ (62 mg, 0.11 mmol) and Hdpf (46 mg, 0.11 mmol) were mixed in dichloromethane (30 mL), and the reaction mixture was stirred overnight. Isolation as described above produced complex $\mathbf{2^{Ph}}$ as an orange solid.

Yield of $2^{Ph}\cdot 1/2CH_2Cl_2$: 65 mg (67%). The crystal of 2^{Ph}·AcOEt used for X-ray diffraction analysis was grown from dichloromethane/ethyl acetate/hexane.

^{1}H NMR (399.95 MHz, $CDCl_3$): δ 3.91 (vq, J' = 2.0 Hz, 2H, fc), 4.13 (vt, J' = 2.0 Hz, 2H, fc), 4.31–4.42 (m, 2H, fc), 5.05 (br vt, J' = 1.8 Hz, 2H, fc), 6.37 (td, J = 7.6, 1.3 Hz, 1H, C_6H_4), 6.65 (ddd with ^{195}Pt satellites, $J_{PtC} \approx 60$ Hz, J = 7.7, 2.2, 1.3 Hz, 1H, C_6H_4), 7.01 (td, J = 7.7, 1.3 Hz, 1H, C_6H_4), 7.12 (ddd, J = 8.2, 1.2, 0.2 Hz, 1H, C_6H_4), 7.31–7.41 (m, 7H, 1H of C_6H_4 and 6H of PPh_2), 7.48–7.61 (m, 6H, 5H of NPh and 1H C_6H_4), 7.65 (dd, J = 7.9, 1.3 Hz, 1H, C_6H_4), 7.80–7.85 (m, 4H, PPh_2), 8.13 (dt, J = 8.3, 0.9 Hz, 1H, C_6H_4).^{13}C{^{1}H} NMR (100.58 MHz, $CDCl_3$): δ 70.67 (s, CH of fc), 71.35 (d, J_{PC} = 7 Hz, CH of fc), 72.73 (s, CH of fc), 75.36 (br d, $^1J_{PC} \approx 55$ Hz, C–P of fc), 75.74 (d, J_{PC} = 10 Hz, CH of fc), 78.97 (s, *C*–COO of fc), 111.83 (s, CH of C_6H_4), 112.59 (s with ^{195}Pt satellites, $J_{PtC} \approx 30$ Hz, CH of C_6H_4), 112.74 (s, CH of C_6H_4), 120.96 (d, $^3J_{PC}$ = 9 Hz, C–N of C_6H_4), 123.39 (s, CH of C_6H_4), 124.13 (s, CH of C_6H_4), 124.23 (d with ^{195}Pt satellites, $J_{PtC} \approx 60$ Hz, J_{PC} = 2 Hz, CH of C_6H_4), 125.19 (s, CH of C_6H_4), 127.94 (s, CH of NPh), 128.23 (d, J_{PC} = 11 Hz, CH of PPh_2), 129.37 (s, CH of NPh), 129.71 (s, CH of NPh), 130.03 (d, $^4J_{PC}$ = 3 Hz, C–N of C_6H_4), 130.43 (d, J_{PC} = 2 Hz, CH of PPh_2), 131.60 (d, $^1J_{PC}$ = 51 Hz, C–P of PPh_2), 134.95 (d, J_{PC} = 12 Hz, CH of PPh_2), 135.36 (s, C–N of NPh), 137.27 (d, $^4J_{PC}$ = 5 Hz, C–N of C_6H_4), 139.89 (d, J_{PC} = 8 Hz, CH of C_6H_4), 148.69 (d, $^2J_{PC}$ = 2 Hz, C–Pt of C_6H_4), 174.27 (s, COO), 178.24 (d, $^2J_{PC}$ = 146 Hz, NCN). ^{31}P{^{1}H} NMR (161.90 MHz, $CDCl_3$): δ 18.9 (s with ^{195}Pt satellites, $^1J_{PtP}$ = 2990 Hz, PPh_2). IR (DRIFTS): ν = 3412 br m, 3054 br m, 1598 s, 1502 m, 1473 m, 1458 s, 1436 m, 1412 m, 1355 m, 1323 s, 1252 w, 1177 m, 1097 m, 1029 m, 921 w, 821 w, 803 w, 772 w, 748 s, 696 s, 645 w, 619 w, 599 w, 538 w, 521 m, 506 s cm^{-1}. HRMS (ESI+) calc. for $C_{42}H_{32}FeN_2O_2PPt$ (M^+): 878.1193, found: 878.1198. Anal. calc. for $C_{42}H_{32}FeN_2O_2PPt\cdot 1/2CH_2Cl_2$ (895.4): C 56.59, H 3.65, N 3.13%. Found: C 56.52, H 3.53, N 2.99%.

X-Ray crystallography

The diffraction data ($\pm h \pm k \pm l$, $\theta_{max} \approx 27.5^\circ$) were collected on a Bruker D8 VENTURE Kappa Duo diffractometer equipped with a PHOTON III detector and a Cryostream Cooler (Oxford Cryosystems) using Mo Kα radiation (λ = 0.71073 Å). The structures were solved by direct methods (SHELXT-2014[29]) and refined by a full-matrix least-squares routine on F^2 (SHELXL-2017[30]). All nonhydrogen atoms were refined with anisotropic displacement parameters. The hydrogen atoms were included in their theoretical positions with their U_{iso}(H) set to a multiple of U_{eq}(C) of their bonding carbon atom (1.2 times for CH and CH_2 groups and 1.5 times for methyl groups). The solvent molecules in the structure of the solvate $2^{Ph}\cdot 1/2$AcOEt were severely disordered in space near the crystallographic inversion centres, and their contribution to the overall scattering was therefore removed using PLATON SQUEEZE.[31] All geometric parameters and structural diagrams were obtained using the PLATON program.[32]

Selected crystallographic data and structure refinement parameters are available in the ESI.† The numerical values were rounded to one decimal place with respect to their estimated standard deviations (ESDs).

DFT computations

The Gaussian 16, Rev. A.03[33] program package was used to perform all quantum chemical calculations and the hybrid functional B3LYP[34] was employed as an established and reliable method to calculate transition metal compounds[35] together with the double-ξ (dz) 6-31G(d)[36] and triple-ξ (tz) 6-311+G(d,p) basis sets.[35,37] Platinum was described by the LANL2TZ ECP and basis set.[38] Dispersion forces were simulated by using the D3 dispersion correction with Becke-Johnson damping (D3BJ).[39] Solvent calculations used the PCM SCRF model and the solvent dichloromethane.[40]

All structures were optimized without any restrictions, employing the default grid (UltraFine). All local minima were verified as true minima by the absence of negative eigenvalues in the vibrational frequency analysis, providing thermochemical data at 298.15 K. If not stated otherwise, all discussed values are the ΔG_{298} values. GaussView[41] and Molden[42] were used for visualization. The coordinates of the optimized structures are available in ESI.†

Orbital composition analysis based on the Natural Atomic Orbitals (NAO)[43] (at the B3LYP(d3bj)/6-311+G(d,p):LanL2TZ(Pt) level of theory) was performed using the Multiwfn software package (version 3.8).[44] Molecular orbitals were visualized using the Avogadro program.[45] Intrinsic bond orbital (IBO) analysis (at the B3LYP(d3)/def2-TZVP:sdd(Pt) level of theory)[46–48] and visualization of the obtained orbitals were performed using IboView software.[49]

Conflicts of interest

There are no conflicts to declare.

Acknowledgements

Financial support for this work was provided through the Institutional Strategy of TU Dresden ''The Synergetic University'' and the Charles University Research Centre program (project UNCE/SCI/014). Computational resources were provided by the e-INFRA CZ project (ID: 90254), supported by the Ministry of Education, Youth and Sports of the Czech Republic. We also thank the ZIH Dresden for allocating computational time to their high-performance computing system.

References

1 For early studies, see: (*a*) R. G. Pearson and D. A. Johnson, *J. Am. Chem. Soc.*, 1964, **86**, 3983; (*b*) K. Saito and K. Masuda, *Bull. Chem. Soc. Jpn.*, 1698, **41**, 384; (*c*) A. J. C. Nixon and D. R. Eaton, *Can. J. Chem.*, 1978, **56**, 1928.

2 J. Vicente and M. T. Chicote, *Coord. Chem. Rev.*, 1999, **193–195**, 1143.

3 (*a*) N. Marion, E. C. Ecarnot, O. Navarro, D. Amoroso, A. Bell and S. P. Nolan, *J. Org. Chem.*, 2006, **71**, 3816; (*b*) N. Marion, P. de Frémont, I. M. Puijk, E. C. Ecarnot, D. Amoroso, A. Bell and S. P. Nolan, *Adv. Synth. Catal.*, 2007, **349**, 2380.

4 (*a*) D. Walther, T. Döhler, N. Theyssen and H. Görls, *Eur. J. Inorg. Chem.*, 2001, 2049; (*b*) S. Rau, K. Lamm, H. Görls, J. Schöffel and D. Walther, *J. Organomet. Chem.*, 2004, **689**, 3582.

5 J.-P. Taquet, O. Siri, P. Braunstein and R. Welter, *Inorg. Chem.*, 2006, **45**, 4668.

6 R. H. Howard, C. Alonso-Moreno, L. M. Broomfield, D. L. Hughes, J. A. Wright and M. Bochmann, *Dalton Trans.*, 2009, 8667.

7 (*a*) S. Richeter, C. Jeandon, R. Ruppert and H. J. Callot, *Chem. Commun.*, 2002, 266; (*b*) S. Richeter, C. Jeandon, J.-P. Gisselbrecht, R. Ruppert and H. J. Callot, *J. Am. Chem. Soc.*, 2002, **124**, 6168.

8 N. Allefeld, J. Bader, B. Neumann, H.-G. Stammler, N. Ignat'ev and B. Hoge, *Inorg. Chem.*, 2015, **54**, 7945.

9 L. Lavaud, Z. Chen, M. Elhabiri, D. Jacquemin, G. Canard and O. Siri, *Dalton Trans.*, 2017, **46**, 12794.

10 (*a*) R. Navarro, J. García, E. P. Urriolabeitia, C. Cativiela and M. D. Diaz de Villegas, *J. Organomet. Chem.*, 1995, **490**, 35; (*b*) O. Cantín, C. Cativiela, M. D. Díaz-de-Villegas, R. Navarro and E. P. Urriolabeitia, *Tetrahedron: Asymmetry*, 1996, **7**, 2695.

11 (*a*) M. Zábranský, I. Císařová and P. Štěpnička, *Eur. J. Inorg. Chem.*, 2017, 2557; (*b*) P. Štěpnička, M. Zábranský and I. Císařová, *J. Organomet. Chem.*, 2017, **846**, 193; (*c*) F. Horký, I. Císařová, J. Schulz and P. Štěpnička, *J. Organomet. Chem.*, 2019, **891**, 44.

12 For similar reactions with Rh(I)-acetylacetonates, see: (*a*) A. Jegorov, B. Kratochvíl, V. Langer and J. Podlahová, *Inorg. Chem.*, 1984, **23**, 4288; (*b*) P. Štěpnička and I. Císařová, *J. Chem. Soc., Dalton Trans.*, 1998, 2807.

13 (*a*) T. G. Appleton, H. C. Clark and L. E. Manzer, *Coord. Chem. Rev.*, 1973, **10**, 335; (*b*) F. R. Hartley, *Chem. Soc. Rev.*, 1973, **2**, 163.

14 (*a*) R. G. Pearson, *Inorg. Chem.*, 1973, **12**, 712; (*b*) J. Vicente, A. Arcas, D. Bautista and P. G. Jones, *Organometallics*, 1997, **16**, 2127.

15 S. Fuertes, A. J. Chueca and V. Sicilia, *Inorg. Chem.*, 2015, **54**, 9885.

16 T. Strassner, *Acc. Chem. Res.*, 2016, **49**, 2680.

17 M. Zábranský, J. Soellner, F. Horký, I. Císařová, P. Štěpnička and T. Strassner, *Eur. J. Inorg. Chem.*, 2019, 2284.

18 (*a*) J. Podlaha, P. Štěpnička, J. Ludvík and I. Císařová, *Organometallics*, 1996, **15**, 543; (*b*) P. Štěpnička, *Eur. J. Inorg. Chem.*, 2005, 3787.

19 These values are larger than $^{1}J_{PtP}$ determined for a $\mathbf{2^{Me}}$-type complex featuring (diphenylphosphino)acetate ligand ($^{1}J_{PtP}$ = 2736 Hz; ref. 17). In addition, the larger $^{1}J_{PtP}$ constant for $\mathbf{2^{Ph}}$ corresponds with the shorter Pt–P bond in this compound: P. G. Waddell, A. M. Z. Slawin and J. D. Woollins, *Dalton Trans.*, 2010, **39**, 8260.

20 O. Bárta, P. Pinter, I. Císařová, T. Strassner and P. Štěpnička, *Eur. J. Inorg. Chem.*, 2020, 575.

21 S. Fery-Forgues and B. Delavaux-Nicot, *J. Photochem. Photobiol. A: Chem.*, 2000, **132**, 137.

22 A. Tronnier, A. Pöthig, S. Metz, G. Wagenblast, I. Münster and T. Strassner, *Inorg. Chem.*, 2014, **53**, 6346.

23 For a description and applications of this approach, see: (*a*) J. Schulz, F. Uhlík, J. M. Speck, I. Císařová, H. Lang and P. Štěpnička, *Organometallics*, 2014, **33**, 5020; (*b*) K. Škoch, I. Císařová, F. Uhlík and P. Štěpnička, *Dalton Trans.*, 2018, **47**, 16082; (*c*) K. Škoch, J. Schulz, I. Císařová and P. Štěpnička, *Organometallics*, 2019, **38**, 3060; (*d*) P. Vosáhlo, J. Schulz, I. Císařová and P. Štěpnička, *Dalton Trans.*, 2021, **50**, 6232.

24 The energy difference between the HOMO and LUMO calculated from the FMO eigenvalues obtained after geometry optimisation are 4.06 eV for $\mathbf{2^{Me}}$, 3.94 eV for $\mathbf{3^{Me}}$, 4.03 eV for $\mathbf{2^{Ph}}$, and 2.88 eV for $\mathbf{3^{Ph}}$.

25 (*a*) G. Knizia, *J. Chem. Theory Comput.*, 2013, **9**, 4834; (*b*) G. Knizia and J. E. M. N. Klein, *Angew. Chem., Int. Ed.*, 2015, **54**, 5518.

26 M. L. H. Green, *J. Organomet. Chem.*, 1995, **500**, 127.

27 R. M. Silverstein, F. X. Webster and D. J. Kiemle, *Spectrometric Identification of Organic Compounds*, Wiley, New York, 7th edn, 2005, ch. 3, p. 127.

28 F. Barrière and W. E. Geiger, *J. Am. Chem. Soc.*, 2006, **128**, 3980.

29 G. M. Sheldrick, *Acta Crystallogr., Sect. A: Found. Adv.*, 2015, **71**, 3.

30 G. M. Sheldrick, *Acta Crystallogr., Sect. C: Struct. Chem.*, 2015, **71**, 3.

31 A. L. Spek, *Acta Crystallogr., Sect. C: Struct. Chem.*, 2015, **71**, 9.

32 (*a*) A. L. Spek, *J. Appl. Crystallogr.*, 2003, **36**, 7; (*b*) A. L. Spek, *Acta Crystallogr. D: Biol. Crystallogr.*, 2009, **65**, 148.

33 M. J. Frisch, G. W. Trucks, H. B. Schlegel, G. E. Scuseria, M. A. Robb, J. R. Cheeseman, G. Scalmani, V. Barone, G. A. Petersson, H. Nakatsuji, X. Li, M. Caricato, A. V. Marenich, J. Bloino, B. G. Janesko, R. Gomperts, B. Mennucci, H. P. Hratchian, J. V. Ortiz, A. F. Izmaylov, J. L. Sonnenberg, D. Williams, F. Ding, F. Lipparini, F. Egidi, J. Goings, B. Peng, A. Petrone, T. Henderson, D. Ranasinghe, V. G. Zakrzewski, J. Gao, N. Rega, G. Zheng, W. Liang, M. Hada, M. Ehara, K. Toyota, R. Fukuda, J. Hasegawa, M. Ishida, T. Nakajima, Y. Honda, O. Kitao, H. Nakai, T. Vreven, K. Throssell, J. A. Montgomery Jr., J. E. Peralta, F. Ogliaro, M. J. Bearpark, J. J. Heyd, E. N. Brothers, K. N. Kudin, V. N. Staroverov, T. A. Keith, R. Kobayashi, J. Normand, K. Raghavachari, A. P. Rendell, J. C. Burant, S. S. Iyengar, J. Tomasi, M. Cossi, J. M. Millam, M. Klene, C. Adamo, R. Cammi, J. W. Ochterski, R. L. Martin, K. Morokuma, O. Farkas, J. B. Foresman and D. J. Fox, *Gaussian 16 Rev. A.03*, Gaussian Inc., Wallingford, CT, 2016.

34 (*a*) A. D. Becke, *Phys. Rev. A*, 1988, **38**, 3098; (*b*) A. D. Becke, *J. Chem. Phys.*, 1993, **98**, 1372; (*c*) A. D. Becke, *J. Chem. Phys.*, 1993, **98**, 5648; (*d*) B. Miehlich, A. Savin, H. Stoll and H. Preuss, *Chem. Phys. Lett.*, 1989, **157**, 200; (*e*) P. J. Stephens, F. J. Devlin, C. F. Chabalowski and M. J. Frisch, *J. Phys. Chem.*,

1994, **98**, 11623; (*f*) S. H. Vosko, L. Wilk and M. Nusair, *Can. J. Phys.*, 1980, **58**, 1200.
35 Y. Zhao and D. G. Truhlar, *Acc. Chem. Res.*, 2008, **41**, 157.
36 (*a*) J.-P. Blaudeau, M. P. McGrath, L. A. Curtiss and L. Radom, *J. Chem. Phys.*, 1997, **107**, 5016; (*b*) R. Ditchfield, W. J. Hehre and J. A. Pople, *J. Chem. Phys.*, 1971, **54**, 724; (*c*) M. M. Francl, W. J. Pietro, W. J. Hehre, J. S. Binkley, M. S. Gordon, D. J. DeFrees and J. A. Pople, *J. Chem. Phys.*, 1982, **77**, 3654; (*d*) M. S. Gordon, *Chem. Phys. Lett.*, 1980, **76**, 163; (*e*) P. C. Hariharan and J. A. Pople, *Theor. Chim. Acta*, 1973, **28**, 213; (*f*) G. A. Petersson, A. Bennett, T. G. Tensfeldt, M. A. Al-Laham, W. A. Shirley and J. Mantzaris, *J. Chem. Phys.*, 1988, **89**, 2193; (*g*) V. A. Rassolov, J. A. Pople, M. A. Ratner and T. L. Windus, *J. Chem. Phys.*, 1998, **109**, 1223; (*h*) M. J. Frisch, J. A. Pople and J. S. Binkley, *J. Chem. Phys.*, 1984, **80**, 3265.
37 (*a*) T. Clark, J. Chandrasekhar, G. W. Spitznagel and P. V. R. Schleyer, *J. Comput. Chem.*, 1983, **4**, 294; (*b*) R. Krishnan, J. S. Binkley, R. Seeger and J. A. Pople, *J. Chem. Phys.*, 1980, **72**, 650; (*c*) A. D. McLean and G. S. Chandler, *J. Chem. Phys.*, 1980, **72**, 5639; (*d*) L. A. Curtiss, M. P. McGrath, J.-P. Blaudeau, N. E. Davis, R. C. Binning and L. Radom, *J. Chem. Phys.*, 1995, **103**, 6104.
38 (*a*) P. J. Hay and W. R. Wadt, *J. Chem. Phys.*, 1985, **82**, 270; (*b*) W. R. Wadt and J. P. Hay, *J. Chem. Phys.*, 1985, **82**, 284; (*c*) P. J. Hay and W. R. Wadt, *J. Chem. Phys.*, 1985, **82**, 299; (*d*) L. E. Roy, P. J. Hay and R. L. Martin, *J. Chem. Theory Comput.*, 2008, **4**, 1029.
39 (*a*) S. Grimme, S. Ehrlich and L. Goerigk, *J. Comput. Chem.*, 2011, **32**, 1456; (*b*) S. Grimme, *Wiley Interdiscip. Rev.: Comput. Mol. Sci.*, 2011, **1**, 211.
40 (*a*) V. Barone and M. J. Cossi, *J. Phys. Chem. A*, 1998, **102**, 1995; (*b*) M. Cossi, N. Rega, G. Scalmani and V. J. Barone, *J. Comput. Chem.*, 2003, **28**, 669; (*c*) J. Tomasi, B. Mennucci and R. Cammi, *Chem. Rev.*, 2005, **105**, 2999.
41 R. D. Dennington, T. A. Keith and J. M. Millam, *Gaussview, version 5.0.8*, Semichem Inc., Shawnee Mission KS, 2009.
42 G. Schaftenaar and J. H. Noordik, *J. Comp.-Aid. Mol. Design*, 2000, **14**, 123.
43 T. Lu and F. Chen, *Acta Chim. Sin.*, 2011, **69**, 2393.
44 T. Lu and F. Chen, *J. Comput. Chem.*, 2012, **33**, 580.
45 (*a*) *Avogadro: An Open-Source Molecular Builder and Visualization Tool, version 1.2.0*, **https://avogadro.openmolecules.net/**; (*b*) M. D. Hanwell, D. E. Curtis, D. C. Lonie, T. Vandermeersch, E. Zurek and G. R. Hutchison, *J. Cheminf.*, 2012, **4**, 17.
46 (*a*) F. Weigend, F. Furche and R. Ahlrichs, *J. Chem. Phys.*, 2003, **119**, 12753; (*b*) F. Weigend and R. Ahlrichs, *Phys. Chem. Chem. Phys.*, 2005, **7**, 3297.
47 (*a*) A. D. Becke and E. R. A. Johnson, *J. Chem. Phys.*, 2005, **123**, 154101; (*b*) S. Grimme, J. Antony, S. Ehrlich and H. A. Krieg, *J. Chem. Phys.*, 2010, **132**, 154104; (*c*) S. Grimme, S. Ehrlich and L. Goerigk, *J. Comput. Chem.*, 2011, **32**, 1456.
48 D. Andrae, U. Haeussermann, M. Dolg, H. Stoll and H. Preuss, *Theor. Chim. Acta*, 1990, **77**, 123.
49 G. Knizia, **https://www.iboview.org**.